

## MEASURING BLADE ANGULAR MOTIONS: A KINEMATICAL APPROACH

Colombo Attilio, Locatelli Alessandro  
Agusta Aeromechanics Department  
Via G. Agusta 520, 21017 Cascina Costa di Samarate, Italy

### Abstract

In recent years Agusta technology of rotor architecture has evolved towards an articulated configuration with elastomeric spherical bearings for the blade retention to the hub and this scheme has been adopted both for the main and the tail rotor on some products. The process of helicopter development and certification, including qualification of the elastomeric bearings, requires the knowledge of the angular components of motion of the blade link that are obtained through deformation of the elastomeric bearing. This knowledge is useful for a variety of scopes, including validation of analytical simulations and codes, flight data analysis, endurance and fatigue test spectra of the elastomeric components.

In order to simplify the mechanical installation layout of the measurement system, an hybrid approach has been developed, where the signals coming from some linear and/or angular displacement transducers are post-processed by an algorithm based on the kinematical relationships imposed by the geometrical arrangement of the hub and measurement system, to extract the desired components of blade angles. This approach has been implemented successfully on a number of different aircrafts, with some variants related to the number and type of sensors that have been used. In this paper a review of the method will be presented, with a discussion of the underlying hypothesis, the tests performed to validate the system and a summary of the results.

### List of symbols

$\zeta$ :	lead-lag angle
$\beta$ :	flap angle
$\theta$ :	pitch angle
$\theta_{\text{COLL}}$ :	collective stick position pitch angle
$\theta_{\text{CYCL}}$ :	cyclic stick position pitch angle
$\theta_{\text{PED}}$ :	pedal position pitch angle
$(*)_0$ :	mean value of the (*) parameter
$(*)_{1\text{REV}}$ :	1 <sub>REV</sub> alternate value of the (*) parameter
$d_i$ :	generic sensor output
$F_C$ :	centrifugal load
$\delta_C$ :	deformation due to the centrifugal load
$U$ :	identity matrix
$R^T$ :	rotational matrix
$e_B$ :	hinge offset

$S_B^\zeta$ :	blade lag static moment respect to the centre of the hub
$S_B^\beta$ :	blade flap static moment respect to the centre of the hub
$\Omega$ :	rotor speed
$K_\zeta$ :	angular lag stiffness
$K_\beta$ :	angular flap stiffness
$K_B$ :	bearing radial stiffness
$K_T$ :	tension link radial stiffness
$\delta_B$ :	bearing deformation due to the centrifugal load
$\delta_T$ :	tension link deformation due to the centrifugal load
$X_M$ :	coordinates of a generic point moving with the mast
$X_P$ :	coordinates of a generic point moving with the blade
$\delta_3$ :	pitch-flap coupling

### Introduction

Articulated rotor configuration with elastomeric spherical bearing has spread over the last Agusta helicopters, both for the main and the tail rotors. The evaluation of the blade angular movements, useful for the development and the certification of the product, is not a trivial task, because of the difficulties to install mechanical sensors measuring the three angles separately. An alternative approach permits to obtain the angular movements starting from other displacements (easily measured by transducers) that are processed by a proper algorithm.

In particular, the attention has been devoted to minimize the number of sensors to be installed, making use, where possible, of already installed ones, like the damper stroke and the tail rotor servo actuator displacement transducer.

The method presented in this work shows a feasible way to perform this task.

### System description

The main hypothesis assumed in this work is that, from a kinematical point of view, the blade root can be considered as a rigid body connected to the hub by means of a spherical hinge (the elastomeric bearing) (Figure 1). As such, it has three angular degrees of freedom (DOF) that can be expressed as

lead-lag ( $\zeta$ ), flap ( $\beta$ ) and pitch ( $\theta$ )<sup>i</sup>. However, other sets of parameters can be chosen as degrees of freedom: it can be shown, for example, that the distances  $d_i$  between three points of the hub and the blade (properly chosen) can univocally define the position of the blade as well. The relation between the two sets of DOF can be formulated by means of some (non linear) transformation,  $L$ :

$$\begin{Bmatrix} d_1 \\ d_2 \\ d_3 \end{Bmatrix} \xrightarrow{L} \begin{Bmatrix} \zeta \\ \beta \\ \theta \end{Bmatrix}$$

$$\begin{Bmatrix} \zeta \\ \beta \\ \theta \end{Bmatrix} \xrightarrow{L^{-1}} \begin{Bmatrix} d_1 \\ d_2 \\ d_3 \end{Bmatrix}$$

The distances  $d_i$  can be experimentally measured by means of appropriate transducers and then processed to provide the position of the blade in terms of  $\zeta, \beta, \theta$  (*direct problem*).

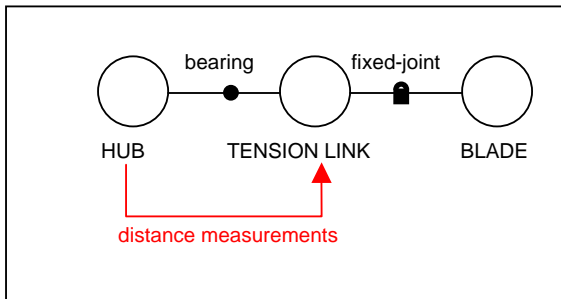


Figure 1 Articulated rotor – link between parts

For each distance measurement  $d_i$  provided by a sensor, an equation in the form:

$$d_i = f(\zeta, \beta, \theta)$$

can be written. This relation is in general non linear, because large angles are allowed.

If the effects of the deformations ( $\delta_c$ ) that the centrifugal load generates on the (elastomeric) bearing and the tension link are included, the relation becomes:

$$d_i = g(\zeta, \beta, \theta, \delta_c)$$

<sup>i</sup> The angles  $\zeta, \beta, \theta$  are defined to be the three sequential rotations around the axis  $z-y'-x''$  of a reference frame moving with the blade (*Euler angles*, see Figure 3).

The following *signum conventions* have been adopted:

- ✓  $\zeta$  (positive with the blade lagging)
- ✓  $\beta$  (positive with the blade rising up)
- ✓  $\theta$  (positive with the profile nose up)

where the symbol  $\delta_c$  indicates that the centrifugal deformation can be evaluated *a priori* and it is not an unknown. If the rotor speed is stabilized, the  $\delta_c$  term is constant and can be evaluated once at the beginning of the computation.

The equation for the  $i^{\text{th}}$ -transducer can be handled in the form:

$$h_i(\zeta, \beta, \theta, \delta_c, d_i) = 0$$

Since the blade angular movements to be evaluated are three, the number of equations (and therefore the number of sensors) must not be less than three.

The non linear system composed by the  $N$  equations represents the mathematical formulation of the *L-transformation*, which solve the *direct problem* (Figure 2).

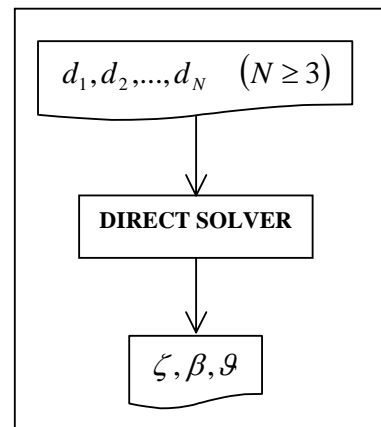


Figure 2 Direct problem

In the present work the number of equation of the system is three ( $N=3$ ). Due to the non linearity of the kinematical equation, it is necessary to take into account the problem of the existence and uniqueness of the solution. In other words, the transformation operator  $L$  shall define a biunique relation between the two  $\mathbb{R}^3$  domains corresponding to the allowable blade angular motions and the sensor measurements.

This property is strongly influenced by a proper location of the sensors: in particular, a geometry of installation where each transducer is mainly sensitive to a single blade angle can satisfy the requirement.

### Kinematical Equations

Let  $X_P^0$  be the coordinates of a point moving with the blade expressed in a blade fixed reference frame with origin on its centre of rotation (i.e. the bearing centre, see Figure 3).

Let  $X_P$  be the coordinates of this point after a generic movement of the blade. It can be written:

$$X_p = R^T(\xi, \beta, \theta) \cdot X_p^0$$

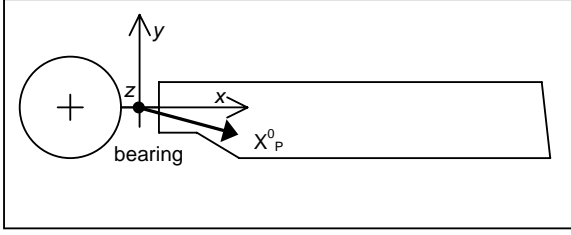


Figure 3 Blade reference frame

where the rotation matrix  $R^T$  is defined as follow:

$$R^T(\xi, \beta, \theta) = T_D^T(\xi) \cdot T_F^T(\beta) \cdot T_P^T(\theta)$$

and:

$$\bullet T_D^T(\xi) = \begin{bmatrix} \cos(\xi) & \sin(\xi) & 0 \\ -\sin(\xi) & \cos(\xi) & 0 \\ 0 & 0 & 1 \end{bmatrix}$$

$$\bullet T_F^T(\beta) = \begin{bmatrix} \cos(\beta) & 0 & -\sin(\beta) \\ 0 & 1 & 0 \\ \sin(\beta) & 0 & \cos(\beta) \end{bmatrix}$$

$$\bullet T_P^T(\theta) = \begin{bmatrix} 1 & 0 & 0 \\ 0 & \cos(\theta) & -\sin(\theta) \\ 0 & \sin(\theta) & \cos(\theta) \end{bmatrix}$$

It can be seen that  $R^T = U$  when  $\xi = \beta = \theta = 0$ .

#### Effect of the centrifugal load

The amplitude of the centrifugal force  $F_c$  is:

$$F_c = S_B^\zeta \cdot \Omega^2$$

with:

- ✓  $S_B^\zeta$  being the *blade lag static moment* respect to the centre of the hub;
- ✓  $\Omega$  being the *rotor speed*.

The deformation due to this load is assumed to be directed along the blade span and is related to the bearing and the tension link flexibility. If  $K_B$  and  $K_T$  are respectively the radial stiffness of the bearing and the tension link, their deformations are:

$$\delta_B = \frac{F_c}{K_B}$$

$$\delta_T = \frac{F_c}{K_T}$$

If the centrifugal effect has to be considered, these terms must be added to the *x-component* of the points on the blade, making:

$$X_p^0 = X_p^0(\delta_c)$$

#### Transducers/Sensors

Sensors allow to get the linear or angular displacement ( $d_i$ ) between two points of the blade and the hub.

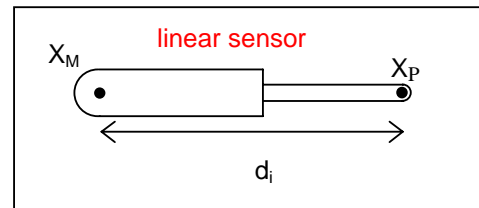
Let

- ✓  $X_M$  be the coordinates of a point attached to the hub;
- ✓  $X_P$  be the coordinates of a point moving with the blade.

The blade movements cause variations in the displacement between  $X_M$  and  $X_P$  that can be measured by the sensors, providing the input to the problem.

Linear or angular displacement transducers can be used, the actual choice depending on the geometrical layout of the hub to be instrumented.

Figure 4 Typical application of a linear sensor



Referring to what said previously, the linear distance between  $X_M$  and  $X_P$  is:

$$d_i = \sqrt{(X_M - X_P)^T \cdot (X_M - X_P)}$$

The expression can be handled as follows:

$$h^{LIN}(\xi, \beta, \theta, \underline{\delta}_c, \underline{d}_i) = \underline{d}_i^2 - |X_M|^2 + |X_P^0(\underline{\delta}_c)|^2 + -2X_M^T R^T(\xi, \beta, \theta) X_P^0(\underline{\delta}_c) = 0$$

In order to reduce the number of additional transducers to be installed on the prototypes, it is possible to make use of existing ones, like the damper stroke measurement sensors.

In case of usage of an angular displacement transducer, the typical layout of the installation is sketched in Figure 5.

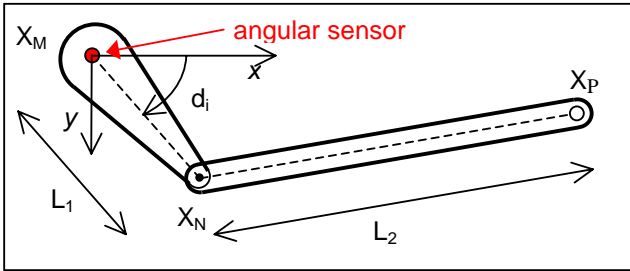


Figure 5 Typical application of an angular sensor

If  $d_i$  is the angular displacement of the transducer due to movement of  $X_P$ , then:

$$\begin{cases} X_N = X_M + L_1 \begin{Bmatrix} \cos(d_i) \\ \sin(d_i) \end{Bmatrix} \\ L_2^2 = (X_N - X_P)^T \cdot (X_N - X_P) \end{cases}$$

This leads to:

$$\begin{aligned} h^{ANG}(\xi, \beta, \theta, \underline{\delta}_c, \underline{d}_i) = & \\ = & |X_M|^2 + L_1^2 + 2L_1 X_M^T \begin{Bmatrix} \cos(\underline{d}_i) \\ \sin(\underline{d}_i) \end{Bmatrix} + |X_P^0(\underline{\delta}_c)|^2 + \\ & - 2 \left( X_M + L_1 \begin{Bmatrix} \cos(\underline{d}_i) \\ \sin(\underline{d}_i) \end{Bmatrix} \right)^T R^T(\xi, \beta, \theta) X_P^0(\underline{\delta}_c) + \\ & - L_2^2 = 0 \end{aligned}$$

#### Installation

The geometrical layout of the installation will be dependent on the actual configuration of the hub to be instrumented. To illustrate the method, a couple of different cases will be presented: the first one can be representative of a main rotor installation, the second one of a tail rotor. They differ in the number and kind of sensors used, as well as the geometry of the installation.

#### Main rotor

In this case, two angular sensors have been employed which are *mainly* sensitive to the pitch and the flap angle variations respectively.

A linear sensor embedded in the main rotor damper has been used. It is *mainly* sensitive to the lead-lag angle variation.

Figure 6 shows schematically the geometry of the installation of the sensors on the main rotor (the red points are connected to the hub, the blue ones to the blade).

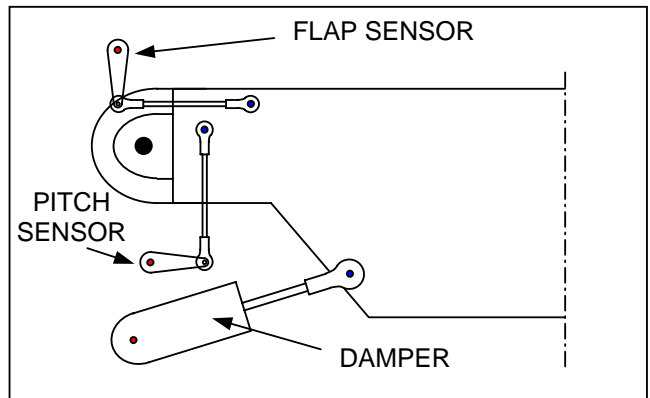


Figure 6 Main rotor – installation of sensors

#### Tail rotor

For the tail rotor, only one additional angular sensor has been employed to measure *mainly* the flap angle variation.

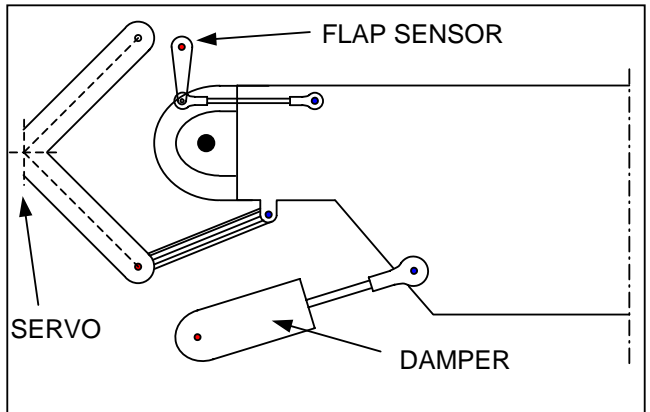


Figure 7 Tail rotor – installation of sensors

Two linear sensors, embedded respectively in the tail rotor damper and in the tail rotor servo actuator, have been used to obtain the lead-lag and the pitch angle variations respectively.

Figure 7 shows a sketch of the installation of the sensors on the tail rotor (the red points are connected to the hub, the blue ones to the blade).

### Numerical algorithm

The numerical algorithm provides the solution of the non-linear system represented by the geometrical relations written for each transducer. It has been used to investigate the issues of biuniqueness of the transformation operator  $L$  and the sensitivity of the solution to the presence of noise into the transducers input data.

As already pointed out, due to the non-linearity of the system it is possible that multiple solutions exist. The investigation lies in solving sequentially an *inverse* and a *direct* problem: starting from an assigned blade angular position  $(\zeta, \beta, \theta)$ , the output of the sensors  $(d_1, d_2, d_3)$  has been recalculated (inverse problem). Then this output becomes the input of the *direct problem* to provide again the blade angular position  $(\zeta, \beta, \theta)$ . These operations are repeated for a large number of times with a random distribution of the angles  $(\zeta, \beta, \theta)$  covering the entire allowable range of blade motions. Comparing the initial imposed set of angles  $(\zeta, \beta, \theta)$  with the recalculated ones, it is possible to test the accuracy of the solution and to verify the uniqueness of the solution.

To investigate the sensitivity to transducer noise, the above process has been modified adding a known distribution of noise (defined as a normal distribution with null mean value and a prescribed standard deviation -  $std_L$  for the noise related to a linear sensor,  $std_R$  for the noise related to an angular sensor) to the calculated transducers signals. The set  $(\zeta, \beta, \theta)$  is now the solution of the noisy problem: the comparison with the initial set  $(\zeta, \beta, \theta)$  leads to an error that must be related to the amplitude of the noise introduced. In this way, it is possible to check if the algorithm amplifies or reduces the noise magnitude.

Figure 8 shows all these steps in a unique flow chart diagram.

Tests have been carried out according to what explained above for typical arrangements of the sensors corresponding to a main and tail rotor configuration, using 1000 sets of three angles (lead-lag, flap, and pitch) chosen at random in their ranges of variation.

For both the main and the tail rotor, for the case without noise no difference between the imposed set of angle  $(\zeta, \beta, \theta)$  and the final one  $(\zeta, \beta, \theta)$  have been found.

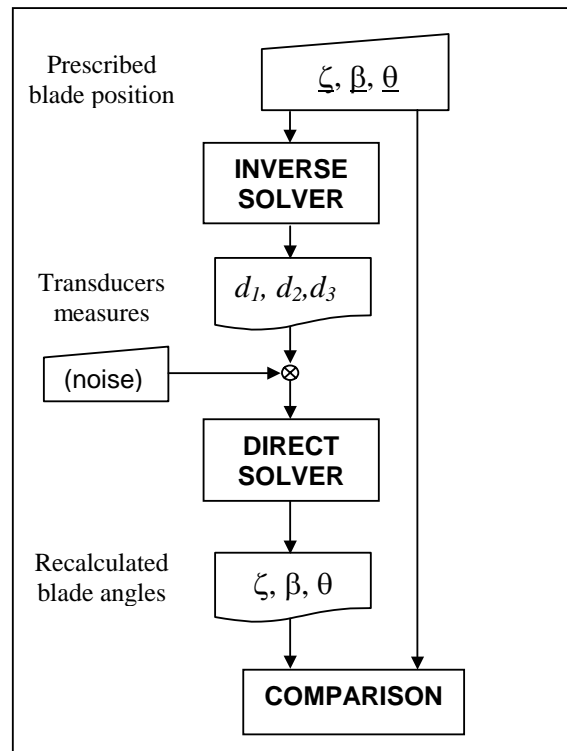


Figure 8 Checking the algorithm – flow chart

These runs have led to some useful considerations: Figure 9 illustrates the relations between a sensor signal and its corresponding blade angle, for the *main rotor* case. It is possible to notice that:

- ✓ the damper and the pitch sensor are *mainly* sensitive to the lead-lag and pitch angle respectively;
- ✓ the flap sensor is influenced by *more than one* blade angle: in fact, for a fixed value of its stroke, a wide range of flap angles are allowed.

To better understand the last statement, it is possible to impose a movement of *one* blade angle throughout its range whilst the *other two* are set to zero and to obtain the signals of the sensors in these conditions by solving the inverse problem. In this way, the effect of *one* angle on *all* the sensors can be seen. The results are shown in Figure 10. It can be noticed that the damper and the pitch sensor are sensitive respectively to a *lead-lag* and *pitch* movement, whilst the flap sensor is sensitive to all the three angles. For this reason, when its stroke is fixed, there are several values of flap angles, corresponding to as many values of lead-lag and flap angles.

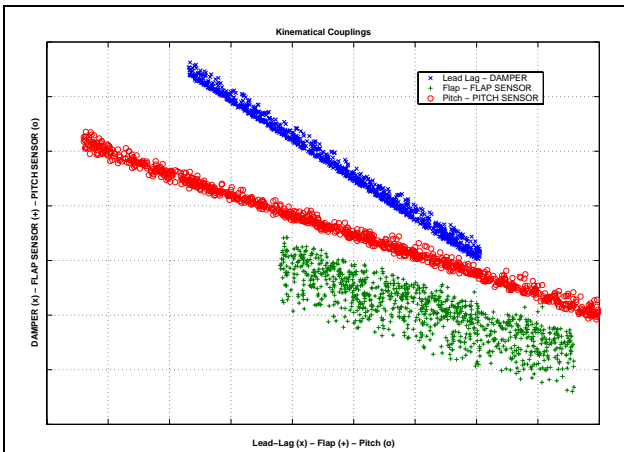


Figure 9 Main rotor – kinematical couplings

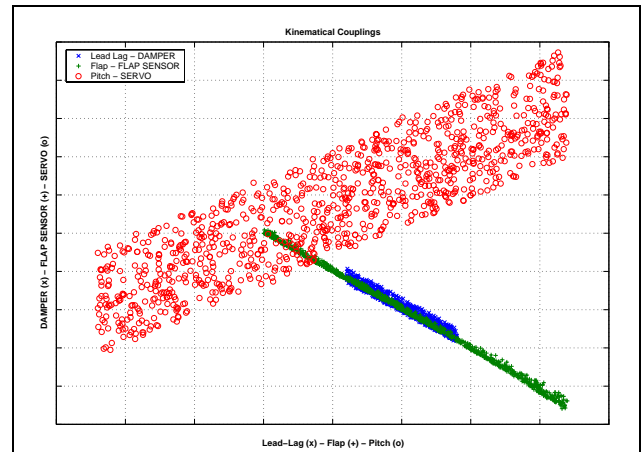


Figure 11 Tail rotor – kinematical couplings

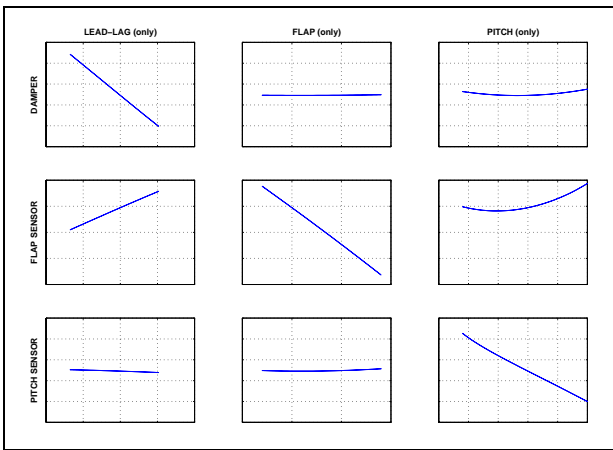


Figure 10 Main rotor – sensitivity matrix

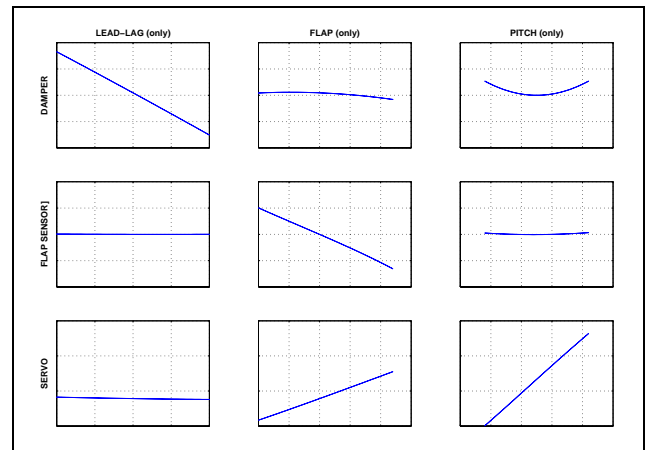


Figure 12 Tail rotor – sensitivity matrix

Analogous remarks can be formulated for the *tail rotor*: Figure 11 shows the relations between a sensor signal and its corresponding blade angle. In this case:

- ✓ the damper and flap sensors are almost entirely sensitive to the lead-lag angle and flap angle and *weakly* sensitive to the other two blade motions values;
- ✓ the signal of the linear sensor placed in the tail rotor servo-actuator is related not only to the pitch motion of the blade but it is coupled also with the other components.

As seen for the main rotor, a *sensitivity matrix* can be built (Figure 12), that shows the relations of the transducers with the blade motions.

It must be noticed that the solver is able to keep into account of all these couplings, without affecting the accuracy of the solution.

For what concerns the *noise sensitivity* evaluation, the test has been carried out in a similar way, with 1000 sets of three angles (lead-lag, flap, and pitch) changing in their ranges of variation in a sinusoidal way.

The noise introduced is a normal distribution with null mean value and a standard deviation equal to 0.5 mm for the linear sensors and 0.5° for the angular sensors.

For the *main rotor* the results are shown in Figure 13: the lines represent the imposed motions and the dots the computed angles when the sensors are affected by the known noise.

Then the *amplitude* of the imposed sensor noise and the *amplitude* of the error are reported in terms of

standard deviation (Table 1) and maximum value (Table 2).

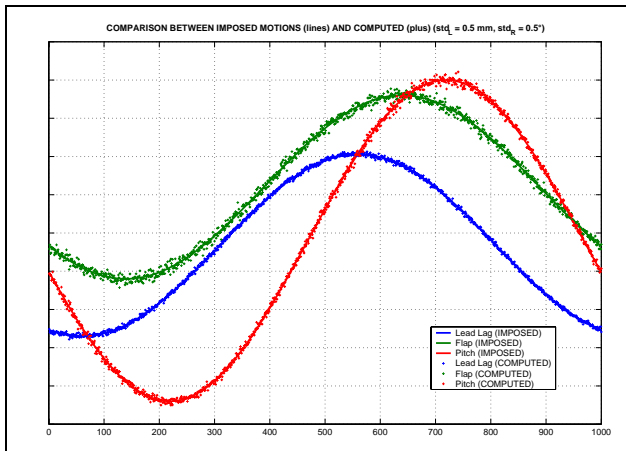


Figure 13 Main rotor (noise sensitivity)

Table 1 Main rotor – input/output errors (standard deviation)

SENSOR	STD	ANGLE	STD
DAMPER	0.4956 mm	LAG	0.1783 °
FLAP SENSOR	0.5131 °	FLAP	0.4059 °
PITCH SENSOR	0.5154 °	PITCH	0.3499 °

Table 2 Main rotor – input/output errors (maximum value)

SENSOR	MAX	ANGLE	MAX
DAMPER	1.5434 mm	LAG	0.6011 °
FLAP SENSOR	1.7876 °	FLAP	1.3314 °
PITCH SENSOR	1.8994 °	PITCH	1.3395 °

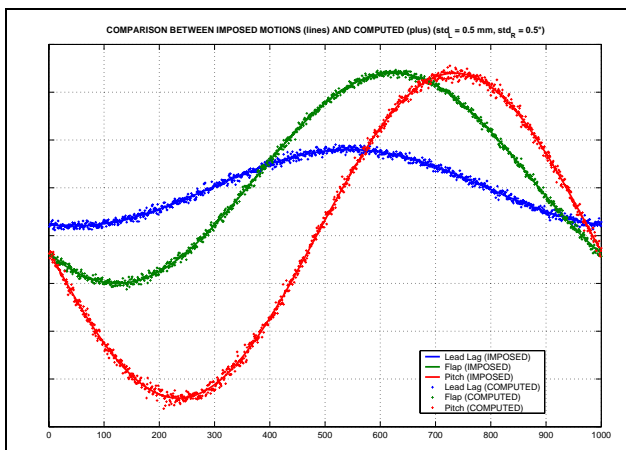


Figure 14 Tail rotor (noise sensitivity)

For the tail rotor, the results are shown in Figure 14: the lines represent the imposed motions and the dots the noisy computed angles.

The amplitude of the imposed sensor noise and the amplitude of the error are listed in Table 3 and Table 4.

Table 3 Tail rotor – input/output errors (standard deviation)

SENSOR	STD	ANGLE	STD
DAMPER	0.5236 mm	LAG	0.2671 °
FLAP SENSOR	0.5054 °	FLAP	0.2459 °
SERVO	0.5039 mm	PITCH	0.3793 °

Table 4 Tail rotor – input/output errors (maximum value)

SENSOR	MAX	ANGLE	MAX
DAMPER	1.7766 mm	LAG	0.8729 °
FLAP SENSOR	2.1075 °	FLAP	0.9622 °
SERVO	1.9293 mm	PITCH	1.4949 °

For both the tail and main rotor, it can be stated that the configurations analysed are not too sensitive to the noise introduced by sensors.

### Validation

A validation of this method has been investigated during some flights carried out with an instrumented helicopter. The outputs of the algorithm (i.e. the blade angles) have been related with appropriate parameters to provide some trends that can be compared with the expected ones. Only steady-state conditions have been considered.

### Collective static pitch angle ( $\theta_0$ )

Both for the main and the tail rotor the average pitch angle can be related with the collective pitch imposed by the pilot, in terms of collective stick position (for the main rotor) and pedal input (for the tail rotor). A significant contribution to the value of  $\theta_0$  is provided by the average flap angle  $\beta_0$ , by means of the  $\delta_3$  coupling.

As for the main rotor, it can be written:

$$\theta_0 = \theta_{COLL} - \beta_0 \tan \delta_3$$

where  $\theta_{COLL}$  is the collective stick position pitch angle.

Figure 15 compares the experimental data points (blue circles) with the expected trend.  $\theta_0$  and  $\beta_0$  have been evaluated by the algorithm and  $\theta_{\text{COLL}}$  comes directly from the instrumentation of the prototype

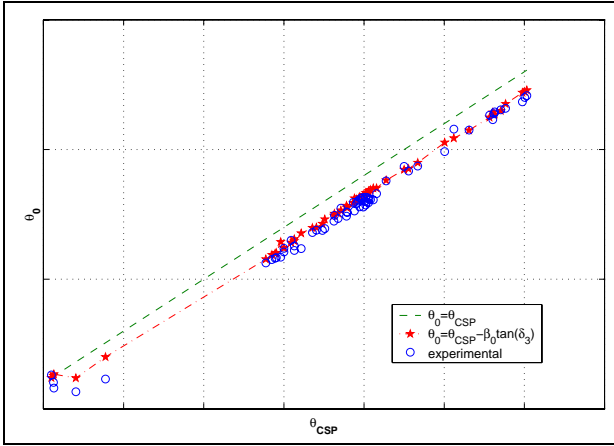


Figure 15 Average main rotor pitch angle versus collective stick position

The green dash line represents the analytical prediction without considering the  $\delta_3$  contribution. As can be seen, it plays an important role in a correct predicting of the actual static (collective) pitch angle.

As for the *tail rotor*, the following similar relation can be found:

$$\theta_0 = \mathcal{G}_{PED} - \beta_0 \tan \delta_3$$

where  $\theta_{\text{PED}}$  is the pedal pitch angle. Figure 16 shows the predicted curves with (red) or without (green) considering the  $\delta_3$  contribution and the experimental one (blue circles).

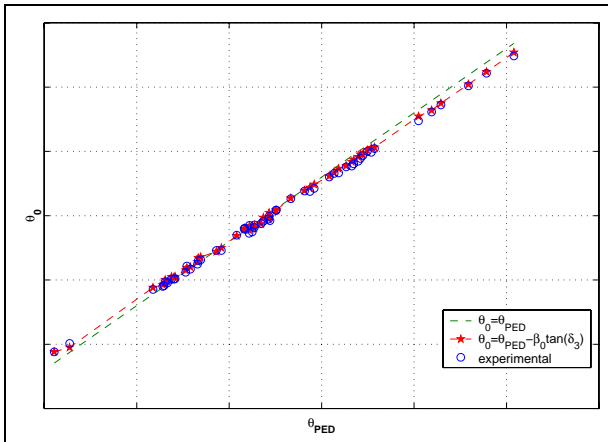


Figure 16 Average tail rotor pitch angle versus pedal position

Also in this case the  $\delta_3$  coupling helps to provide a more accurate estimation of the collective pitch angle, even if its contribution is smaller, because of the smaller values of cone angle with respect to the main rotor.

Dynamic pitch angle at 1<sub>REV</sub> ( $\theta_{1\text{REV}}$ ).

The 1<sub>REV</sub> oscillating pitch angle is strictly related to a cyclic stick input ( $\theta_{\text{CYCL}}$ ) and to the 1<sub>REV</sub> flap angle ( $\beta_{1\text{REV}}$ ), by means of the  $\delta_3$  coupling.

As for the *main rotor*, both the contributions exist, but, since the greatest one comes from the cyclic control input, the  $\delta_3$  coupling is not considered, leading to:

$$\mathcal{G}_{1\text{REV}} = \mathcal{G}_{\text{CYCL}}$$

where  $\theta_{\text{CYCL}}$  is the total cyclic input, due to both the lateral and longitudinal input.

Figure 17 shows the cross-plot of these entities: it can be seen that there is a linear trend as expected, but there is also some deviations that can be attributed to the  $\delta_3$  effect not considered.

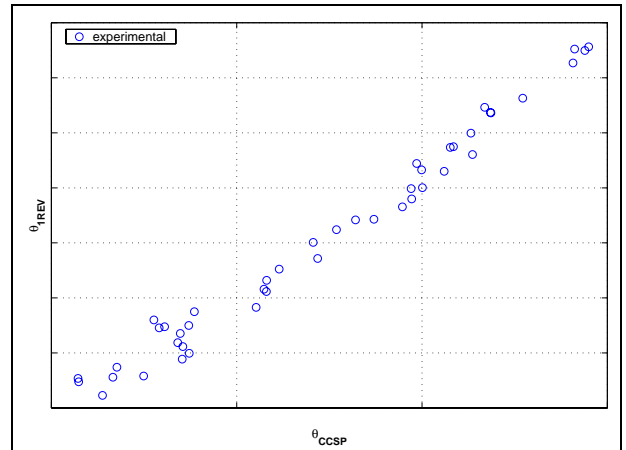


Figure 17 1rev dynamic main rotor pitch angle versus total cyclic stick position

As for the *tail rotor*, the problem is simpler, because of the absence of a cyclic control input, leading to the following relation:

$$\mathcal{G}_{1\text{REV}} = \beta_{1\text{REV}} \tan \delta_3$$

Figure 18 shows the cross-plot of these entities, as obtained by the flight data.

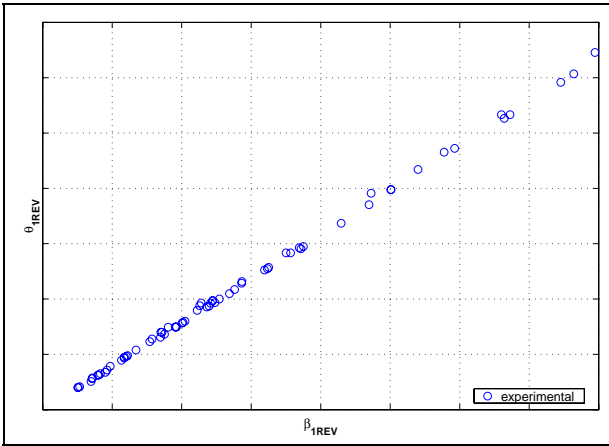


Figure 18 1rev tail rotor pitch angle versus 1rev alternate tail rotor flap angle

The slope of this curve is found to be very close to the tangent of  $\delta_3$ , as expected by analysis.

Static lead-lag angle ( $\zeta_0$ ).

The mean torque  $TQ_0$  can be assumed to be proportional to the mean lead-lag angle, according to the following relation:

$$TQ_0 = (e_B S_B^\zeta \Omega^2 + K_\zeta) \cdot \zeta_0$$

where:

- ✓  $e_B$  is the hinge offset;
- ✓  $S_B^\zeta$  is the blade lag static moment referred to the hub;
- ✓  $\Omega$  is the rotor speed;
- ✓  $K_\zeta$  is the lag stiffness due to the elastomeric bearing cocking spring rate.

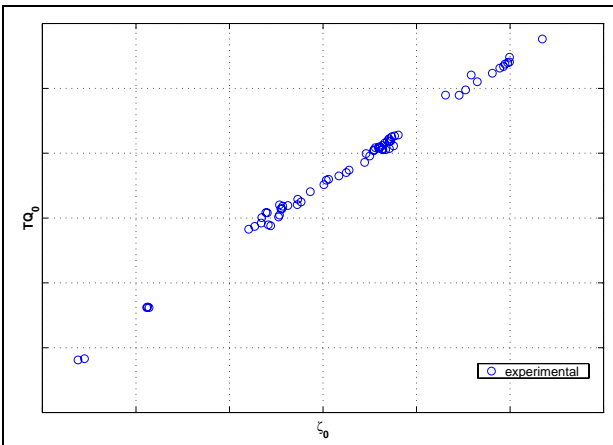


Figure 19 Average main rotor mast torque versus average main rotor lead-lag angle

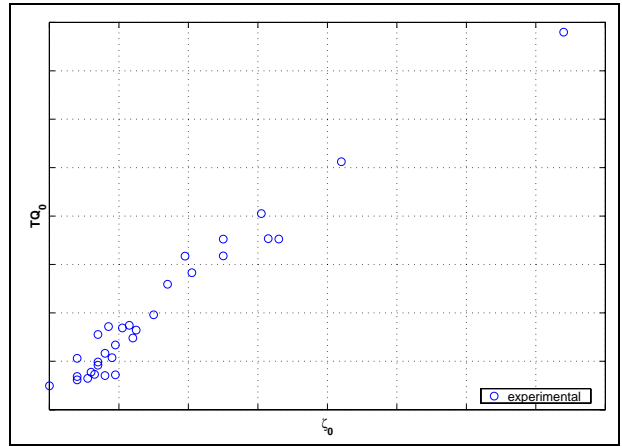


Figure 20 Average tail rotor mast torque versus average tail rotor lead-lag angle

The terms in the bracket can be evaluated in order to provide an analytical estimation of the slope of the line.

The equation is valid for the *main rotor* (Figure 19) and the *tail rotor* (Figure 20) and the experimental slopes are close to the analytical ones.

Dynamic flap angle at  $1_{REV}$  ( $\beta_{1REV}$ )

The  $1_{REV}$  main rotor mast control moment can be assumed to be proportional to the  $1_{REV}$  flap angle according to the relation:

$$M_{1REV}^c = \frac{N_B}{2} (e_B S_B^\beta \Omega^2 + K_\beta) \cdot \beta_{1REV}$$

where:

- ✓  $e_B$  is the hinge offset;
- ✓  $S_B^\beta$  is the blade flap static moment referred to the hub;
- ✓  $\Omega$  is the rotor speed;
- ✓  $K_\beta$  is the elastomeric bearing cocking spring rate.

The term in the bracket, representing the slope of the line, can be evaluated and compared with the one obtained by flight data.

The equation is valid for both the rotors (Figure 21 and Figure 22): it can be seen that the experimental slopes are quite close to the estimated ones.

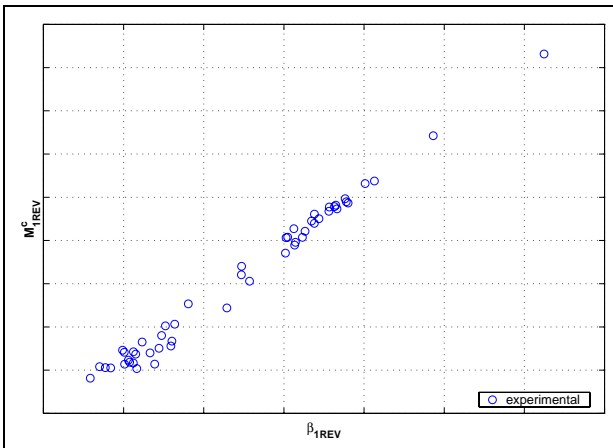


Figure 21  $1_{REV}$  main rotor mast control moment versus  $1_{REV}$  main rotor flap angle

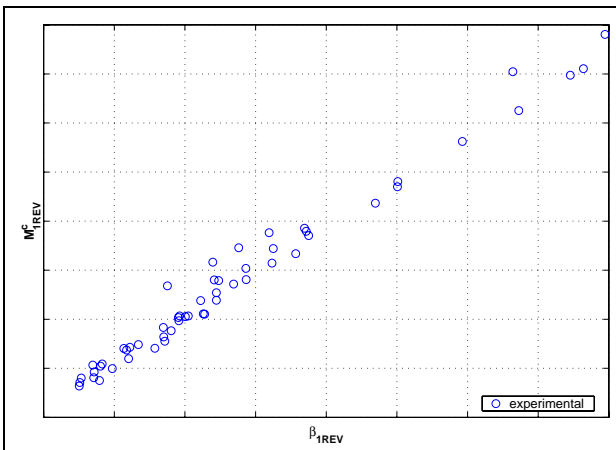


Figure 22  $1_{REV}$  alternate tail rotor mast control moment versus  $1_{REV}$  alternate tail rotor flap angle

### Conclusions

A kinematical method to compute the *lead-lag*, *flap* and *pitch* angles of rotor blades has been presented. It is based on the installation of a proper set of displacement transducers between the hub and the blade. The measure of these sensors are processed by a numerical algorithm to extract the desired blade angles.

The number of sensors can be minimized by making use of already installed instrumentation.

The main hypothesis underlying the method are:

- ✓ the blade root is considered as a rigid body connected to the hub by means of a spherical hinge;
- ✓ the centrifugal force acting on the elastomeric bearing and the tension link produces only an axial deformation of these items;

- ✓ the kinematical constraint equation includes all the non linear effects associated to large rotations.

The mathematical algorithm for solving the non-linear system has been investigated, in order to show that the solution can always be univocally found and that the noise introduced by sensors is not amplified.

A validation of the results can be achieved by correlating the prototype blade angles with other parameters normally recorded during flights.

These relations can be used to provide an estimation of blade angles even when the sensors are not installed.